Observing Chemical and Morphological Changes in a Cu@TiO_x Core@Shell Catalyst: Impact of Reversible Metal-Oxide Interactions on CO₂ Activation and Hydrogenation

Kaixi Deng^{1, 2}, Xiaobo Chen³, Jorge Moncada², Kenna L. Salvatore¹, Ning Rui², Wenqian Xu⁵, Shuting Xiang⁴, Nebojsa Marinkovic⁶, Anatoly I. Frenkel^{2, 4}, Guangwen Zhou³, Stanislaus S. Wong¹, José A. Rodriguez*^{1,2}

- 1. Department of Chemistry, Stony Brook University, Stony Brook, NY 11794, USA 2. Chemistry Division, Brookhaven National Laboratory, Upton, NY 11973, USA
- 3. Program of Materials Science and Engineering, Department of Mechanical Engineering, State University of New York at Binghamton, NY 13902, USA
 - 4. Materials Science and Chemical Engineering Department, Stony Brook University, Stony Brook, NY 11794, USA
- 5. X-ray Science Division, Advanced Photon Source, Argonne National Laboratory, Lemont, Illinois 60439, USA
 - 6. Synchrotron Catalysis Consortium, Columbia University, New York, NY 10027, USA
 - * Corresponding author, E-mail: rodrigez@bnl.gov

Abstract

A combination of several *in-situ* techniques (XRD, XAS, AP-XPS, E-TEM) was used to explore links between the structural and chemical properties of a Cu@TiO_x catalyst under CO₂ hydrogenation conditions. The active phase of the catalyst involved an inverse oxide/metal configuration, but the initial core@shell motif was disrupted during the pre-treatment in H₂. As a consequence of strong metal-support interactions, the titania shell cracked and Cu particles migrated from the core to on top of the oxide with the simultaneous formation of a Cu-Ti-O_x phase. The generated Cu particles had a diameter of 20-40 nm and were decorated by small clusters of TiO_x (< 5 nm in size). Results of in-situ XAS and XRD and images of E-TEM showed a very dynamic system, where the inverse oxide/metal configuration promoted the reactivity of the system towards CO₂ and H₂. At room temperature, CO_2 oxidized the Cu nanoparticles ($CO_{2,gas} \rightarrow CO_{gas} + O_{oxide}$) inducing a redistribution of the TiO_x clusters and big modifications in catalyst surface morphology. The generated oxide overlayer disappeared at elevated temperatures (> 180 °C) upon exposure to H₂, producing a transient surface that was very active for the reverse water-gas shift reaction ($CO_2 + H_2 \rightarrow CO + H_2O$) but was not stable at 250 °C. When oxidation and reduction occurred at the same time, under a mixture of CO₂ and H₂, the surface structure evolved toward a dynamic equilibrium that strongly depended on the temperature. Neither CO₂ nor H₂ can be considered as passive reactants. In the Cu@TiO_x system, morphological changes were linked to variations in the composition of metal-oxide interfaces which were reversible with temperature or chemical environment and affected the catalytic activity of the system. The present study illustrates the dynamic nature of phenomena associated with the trapping and conversion of CO₂.

Keywords: Surface reactions; Surface Microscopy; Catalysis; CO₂ hydrogenation; Copper; Titanium dioxide

Introduction

Nowadays, the trapping and conversion of CO₂ is a major issue in environmental chemistry. 1,2,3,4 Metal-oxide interfaces are frequently used for the catalytic conversion of CO₂ into into fuels and high-value chemicals. 5,6,7,8,9,10,11,12 There have been a lot of studies focused on identifying the active phase of metal/oxide catalysts that are active for the hydrogenation of CO₂ to methanol. 7-11,13 High-resolution transmission electron microscopy (HR-TEM) has been used to study the morphology of powder Cu/ZnO/Al₂O₃ catalysts after exposure to pure H₂ or the CO₂/H₂ reactants.^{9,10} The microscopy results showed that the active phase of the catalyst involved an inverse oxide/metal configuration produced as a consequence of strong metal-support interactions. ^{9,10} The addition of ZnO to copper opens new reaction channels for the dissociation of H₂ and conversion of CO₂ to CO or oxygenates.^{7,14,15} Cu-TiO₂ interfaces also display superior activity and selectivity during CO_2 hydrogenation and are receiving a lot of attention. 16,17,18,19,20,21 They can exhibit a lot of interesting features. 16-22,23 In particular, the trapping of Cu centers into the titania lattice can prevent admetal sintering and improve long term activity and stability for CO₂ hydrogenation. ²⁰ Furthermore, the formation of Cu-Ti-O_x units can facilitate H₂ dissociation and the hydrogenation of CO₂ into oxygenates. ^{21,23} Recent theoretical calculations have predicted that a Cu/TiO₂ interface binds CO₂ much better than isolated copper or titania, ²² and spontaneous dissociation of CO₂ to CO has been observed on defective surface of Cu(I)/TiO_{2-x} nanoparticles at room temperature. ¹⁷ In this article, we use a combination of in-situ techniques {X-ray absorption spectroscopy (XAS), X-ray diffraction (XRD), X-ray photoelectron spectroscopy (XPS), and environmental transmission electron microscopy (E-TEM)} to examine in detail the chemical and structural evolution of a Cu@TiOx core@shell catalyst under CO2 and CO2 hydrogenation conditions.¹⁹ As in the case of Cu/ZnO/Al₂O₃,^{9,10} we find an active phase with an inverse

oxide/metal configuration, but, in addition, our E-TEM images show that there are large structural and morphological changes in the catalyst as a consequence of CO₂ or H₂ dissociation and these changes are completely reversible with temperature and chemical environment.

The phenomenon of metal-support interactions (MSIs) has received much attention and research since its discovery, ²⁴ as it has a significant impact on the structural and chemical properties of a catalyst, thereby determining its performance.^{25,26,27} It can go all the way from changes in the chemical properties produced by electronic perturbations associated with the bonding of a metal and a substrate²⁸ to large structural changes like the encapsulation of a noble metal by an oxide support. 9,10,23,29,30 In principle, the nature of a metal-support interaction changes when the chemical properties of the metal or support evolve. 24-28 Encapsulation of a metal by an oxide is a very important type of MSI. 9,10,21-15,29,30 As noble metals have a relatively high surface energy and work function, forming an oxide layer on the metal particles could lower the surface energy of the catalysts and stabilize a partially reduced oxide. 24-27,31,32 Copper has a relatively lower surface free energy but encapsulation of this metal has been seen in the case of Cu/ZnO/Al₂O₃ and Cu@TiO_x catalysts.^{9,10,19} When dealing with inverse oxide/copper, or core(copper)@shell(oxide) structures, the morphology of the system may be more dynamic than in the case of a noble metal like Pt because copper has higher oxide formation enthalpies.³³ Thus, the Cu-TiO₂ and CuO-TiO₂ pairs form Cu-Ti-O_x solid solutions that can enhance the catalytic performance of the system^{18-21,31}

In the present study, thanks to a multi-technique approach, a correlation between the evolving Cu@TiO_x structure and its CO₂ hydrogenation activity is established. An inverse oxide/metal configuration plays a central role in the reactivity of the system towards CO₂ and H₂, making possible dynamic changes in surface morphology that are reversible when the temperature

is switched between 25 and 350 °C. The observed behaviors are distinct from the classical noble metal core@shell structures where the dynamics are mostly observed in the shell part.³⁴ In our work, important insights have been obtained from transient studies, which are not readily achievable by any other means. Significantly, we have obtained a full understanding of the catalyst's prevailing structure under normal operation conditions, which cannot be extracted from conventional steady state experiments. These results illustrate the dynamic nature of structural changes linked to the binding and conversion of CO₂.

Results and Discussion

A. Reaction with H₂ and O₂: Changes in chemical state and morphology

Inspired by the inverse oxide/metal configuration found for the active phase of $Cu/ZnO/Al_2O_3$ catalysts, 9,10 we tried to generate such a configuration for $Cu-TiO_2$ by synthesizing $Cu@TiO_x$ core-shell structures. 19 Indeed, TEM images for the fresh $Cu@TiO_2$ systems showed a configuration where nanowires (NWs) of copper were covered by a shell of titania. 19 A typical result is shown in **Figure 1a**. In XAS and XPS, the main species detected were Ti^{4+} and Cu^0 plus copper partially oxidized ($Cu^{\delta+}$) at the metal-oxide interface. 19

In this study, before doing any catalytic test, we investigated the stability of these Cu@TiO_x core-shell structures under the standard pre-treatment in O₂/H₂ used for CO₂ hydrogenation catalysts, ^{8,11,12,19} following the behavior of the sample with a combination of XRD, XAS, AP-XPS and TEM. Treatment in O₂ at 350 °C induced a migration of Cu into the titania to form a Cu-Ti-O_x solid solution^{20,21,23,31} and the characteristic diffraction lines of Cu or TiO₂ in XRD disappeared (**Figure 1d**). An extreme case of a Cu-Ti-O_x solid solution is a copper titanate (CuTiO₃) perovskite.³¹ The mixed-metal oxide generated by the oxidation of the Cu@TiO_x coreshell structures did not transform into this compound and remained mainly amorphous in XRD

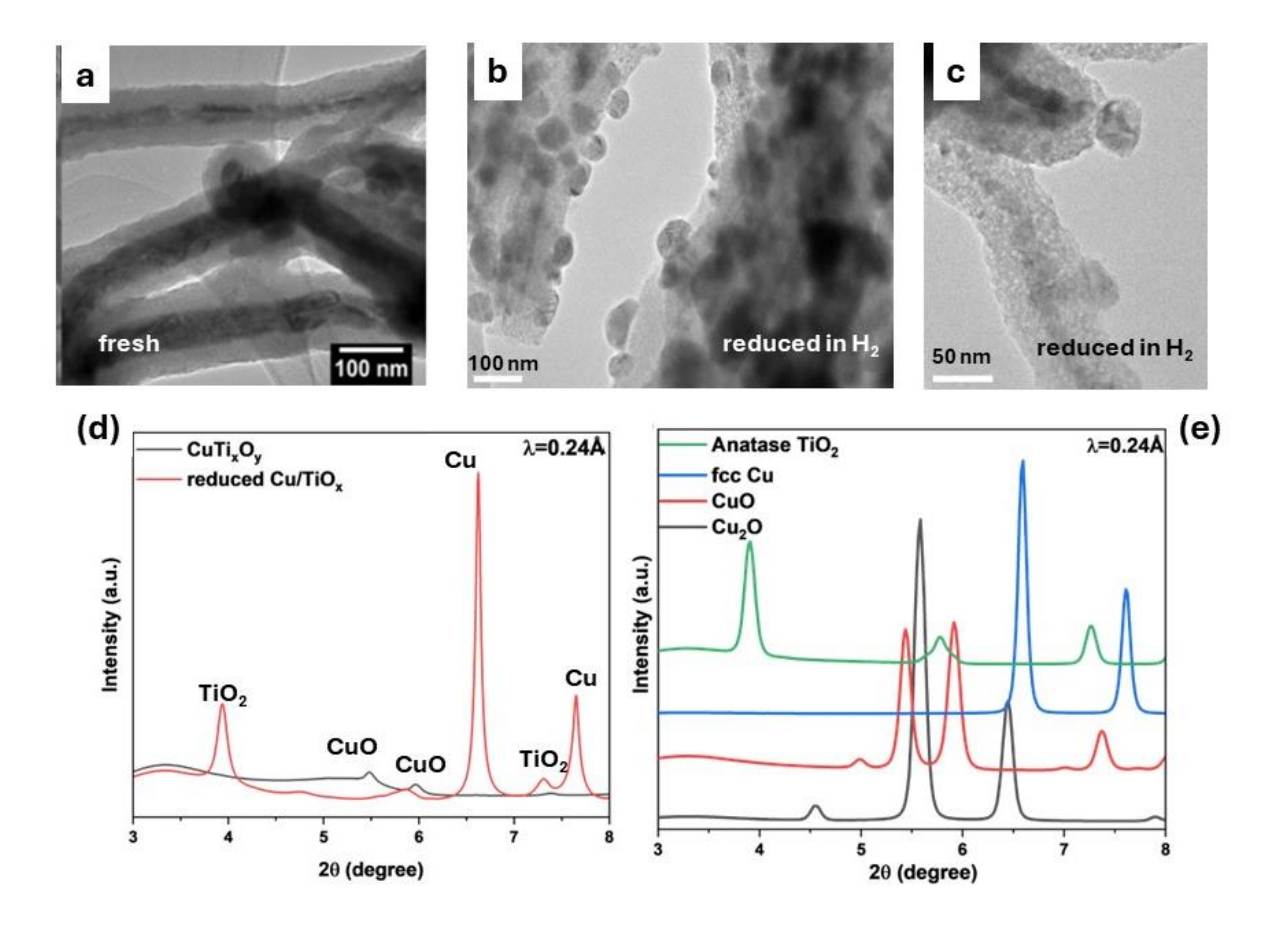


Figure 1. (a) TEM image from a fresh Cu@TiO₂ core shell catalyst. Taken from ref 19 with permission. Copyright 2020 by American Chemical Society. (**b,c**) TEM images for a sample prepared by calcining the core@shell nanowires in $10\%O_2/N_2$ at 350 °C for 1 h followed by reduction in 50% H₂/N₂ at 450 °C for 1 h. (**d**) XRD of a CuTi_xO_y solid solution, prepared by calcining the core@shell nanowires in $10\%O_2/N_2$ at 350 °C for 1 h, along with a Cu/TiO_x sample prepared by reducing the CuTi_xO_y in 50% H₂/N₂ at 450 °C for 1 h. (**e**) XRD diffraction patterns of several standards.

with some weak diffraction lines for CuO (**Figure 1d**). Subsequent exposure to H_2 at high temperatures (> 250 °C) led to a reduction of $Cu^{\delta+}$ cations in the Cu-Ti-O_x solid solution and diffraction lines for Cu and anatase were detected (**Figure 1d**). At this point, TEM images showed a disruption of the initial core@shell configuration with the titania shell cracking and Cu particles migrating from the core to the top of the oxide (**Figure 1b,c**).

Figure 2 shows images coming from high-angle annular dark field (HAADF) and energy-dispersive X-ray spectroscopy (EDS) measurements for a pre-reduced Cu@TiO_x catalyst. Copper exists in three forms in the sample: (i) as a nanowire encapsulated by a TiO₂ shell of about 50 nm

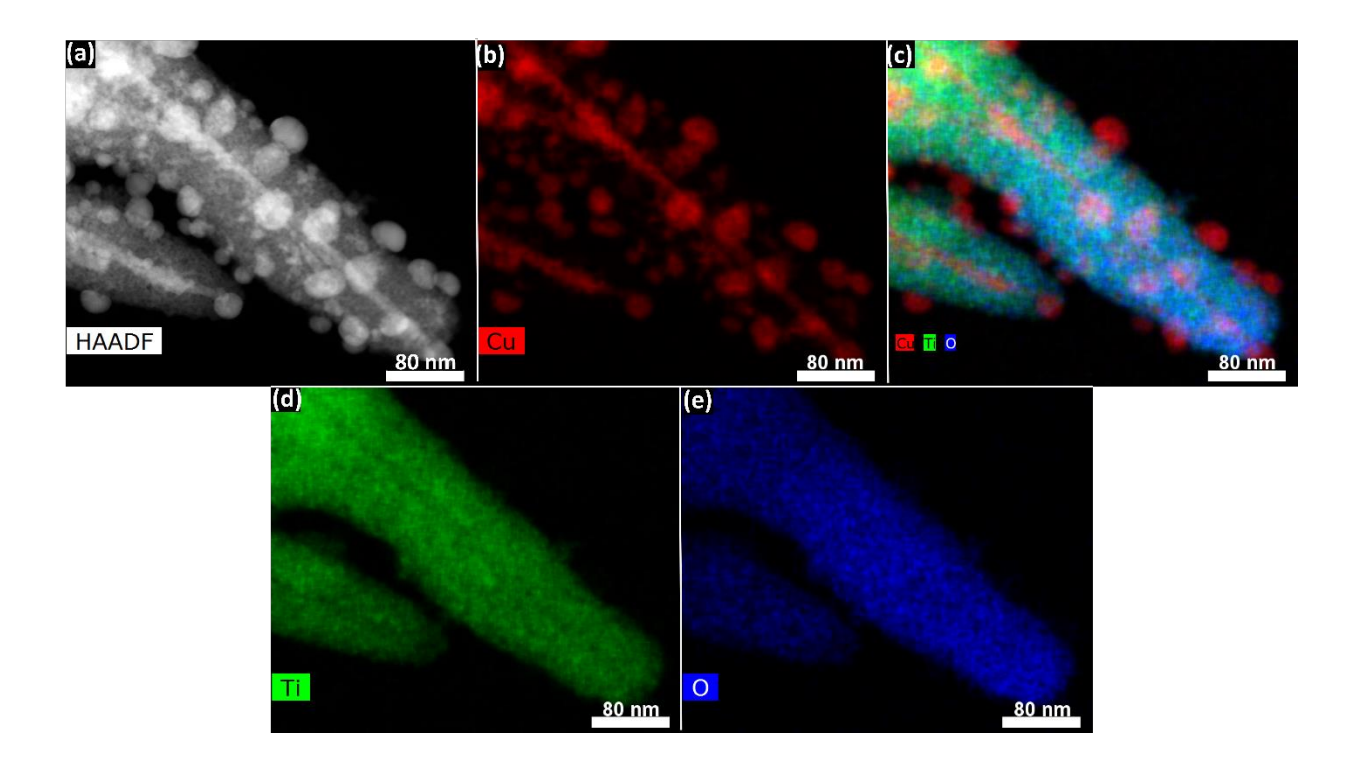


Figure 2. Characterization of a pre-reduced $Cu@TiO_x$ sample using HAADF (a) and EDS elemental mapping (c-e), The images were collected ex-situ after performing H_2 treatment at 450 °C.

in thickness, (ii) as particles of 20-40 nm in diameter on the surface of TiO_2 , and (iii) as a component in a Cu-Ti-O_x mixed oxide. This assertion is in agreement with previous studies for the reduction of the Cu@TiO₂ system.¹⁹ As we will see below, the generated Cu particles and the aggregates of TiO_x or Cu-Ti-O_x phase define the structural and catalytic properties of the system under different chemical environments.

In **Figure 3**, we focus on the properties of a Cu particle supported on titania that has been reduced (top two rows of data) and then exposed to O_2 at room temperature (bottom row). The panels in the top half display E-TEM images for a system that is under 5 mTorr of H_2 at 450 °C. The corresponding results of AP-XPS spectra (**Figures 3b,c** and **S1**) indicate that this system contains metallic copper and $TiO_{1.97}$. This finding is consistent with the results of EELS imaging ($Ti L_{2,3}$ and $Cu L_3$ edges) where one can see particles of copper over a titania substrate. The EELS results also show the existence of small clusters of TiO_x (< 5 nm in size) on top of the copper particles (**Figures 3** and **S3**). Thus, in some areas there is an inverse oxide/metal configuration as seen for either $ZnO/Cu^{9,10}$ or the TiO_x/Pt and TiO_x/Ni systems after exposure to hydrogen. The results of XPS (**Figures 3c and S1b**) and XAS (**Figure S2**) indicate that the amount of Ti^{3+} present in the reduced $Cu@TiO_x$ is not large (< 5% of the Ti cations). This is not surprising since titanium oxides are not easy to reduce at temperatures below 500 °C. 35, 36

For comparison, at the bottom of **Figure 3** are shown results that come from a sample partially oxidized by O_2 at room temperature. On top of the Cu particle, there was an accumulation of oxygen and a redistribution of the TiO_x clusters. This was a common result seen on the copper particles (**Figures 3 and S3**). In general, we found that the reduced samples were oxidized when they were exposed to O_2 at temperatures between 25 and 350 °C, with the typical satellites for Cu^{2+} found in XPS measurements (**Figure S4**). The higher the temperature, the faster the oxidation process and the bigger the amount of copper oxide formed. In an extreme case, after exposure to a very large amount of O_2 at high temperature, a complete $Cu@TiO_x \rightarrow CuO/Cu-Ti-O_x$ transformation was seen with disappearance of the long-range order in the system (**Figure 4**) and the diffraction lines for Cu and TiO_2 (**Figure 1c**).

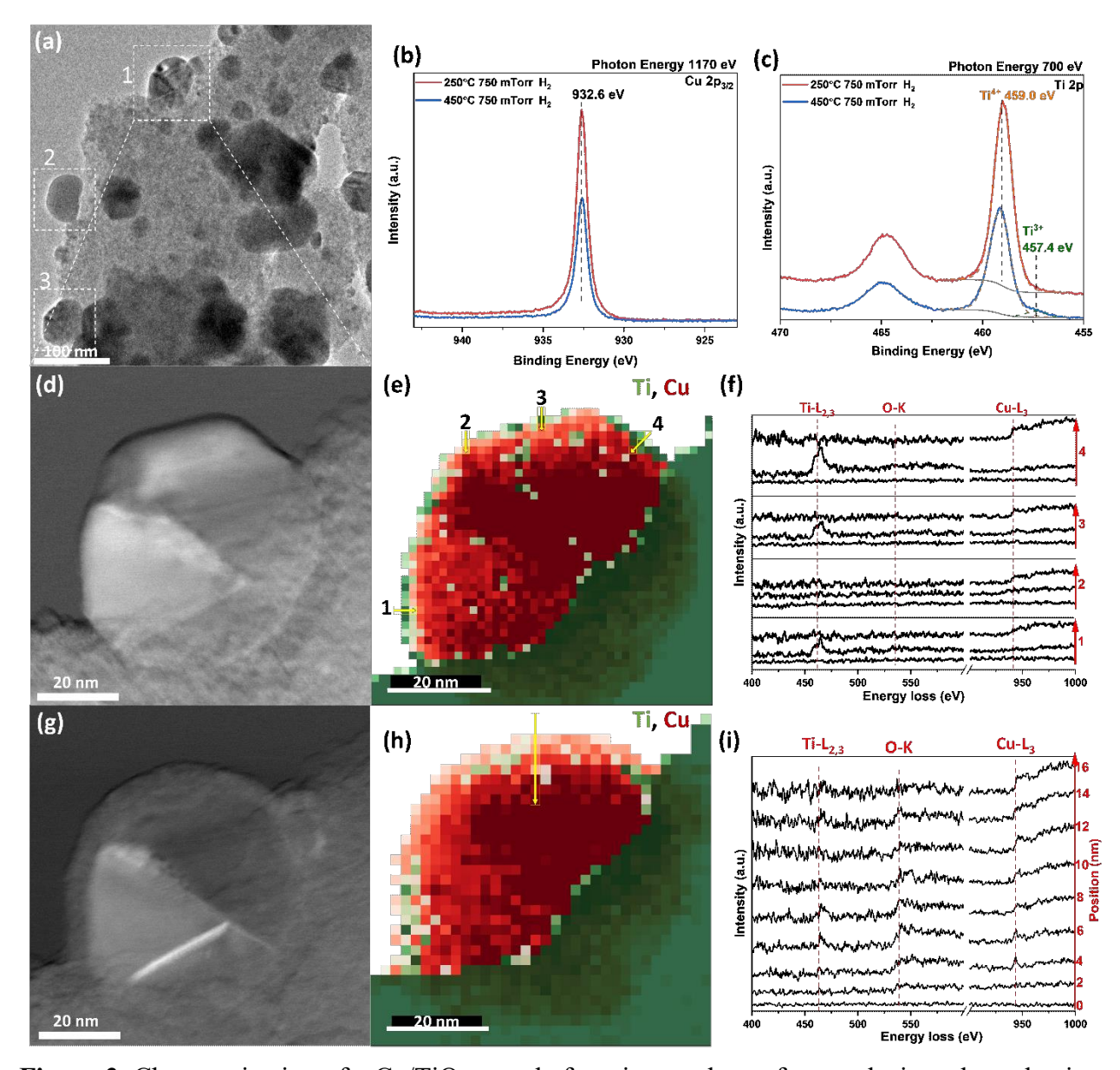


Figure 3. Characterization of a Cu/TiO₂ sample focusing on the surface analysis under reduction and oxidation conditions. (a) Transmission electron microscopy (TEM) image of the sample under a 450°C, 5 mTorr H₂ environment. (b-c) AP-XPS spectra for the Cu 2p_{3/2} (b) and Ti 2p (c) regions of a sample exposed to 750 mTorr of H₂ at 250 or 450 °C. (d-f) Scanning transmission electron microscopy-electron energy loss spectroscopy (STEM-EELS) analysis of a particle {"1" indicated by the white dashed square in (a)} under a 450°C, 5 m of Torr H₂, (g-i) room temperature background oxygen oxidation. Annular dark-field (ADF) images (d,g), combined EELS mappings for Ti-L_{2,3} (green) and Cu-L₃ (red) features (e,h). The pixel size in (e) is 1.5 x 1.5 nm, and in (h), it is 2 x 2 nm. The EELS spectra for Ti-L_{2,3}, O-K, and Cu-L₃ edges are shown at (f) [line positions 1-4 in (e)] and at (i) [the yellow line in (h)]. The corresponding analysis for the particles labeled "2" and "3" in panel (a) is shown in **Figure S3.**

Using E-TEM, we investigated process of oxidation in O₂ (Figure S4) and reduction in H_2 (Figure S5) for the Cu@TiO_x catalyst. The images are consistent with Cu \rightarrow CuO_x ^{38,39} and/or Cu/TiO_x \rightarrow Cu-Ti-Ox ^{23,31,36} transformations in the presence of O₂. The existence of Cu-Ti-O_x units could accelerate the oxidation of the system when it is exposed to O₂ (or CO₂). 20,31,36 In agreement with the XRD results in Figure 1e, an amorphous structure is seen in the TEM images for the formed CuOx/Cu-Ti-Ox phases (Figure S4). In the Ti K-edge XAS for the oxidized Cu@TiO_x (Figure S2), one finds features that are not seen for pure phases of titania (anatase, rutile or brookite), 40,41,42 but appear when this oxide is doped with a second metal. 43,44 This is consistent with the idea that part of the copper goes into the titania lattice to form a Cu-Ti-O_x mixed oxide. ^{20,21,31,36} In Figure **S4**, there is a loss of long range crystallinity that can be reverted if the sample is exposed to hydrogen at elevated (> 200 °C) temperatures (Figures 1d and S6). It is well known that copper oxides undergo fast reduction when exposed to H₂ at temperatures above 200 °C. 15,45,46,47,48 The images in **Figure S5** point to a continuous change in the surface morphology during the reduction process. Amorphous structures associated with TiO_x or Cu-Ti-O_x remain, but the features for pure Cu₂O are removed. There is a redistribution of Ti species on the Cu surface: A TiO_x or Cu-Ti-O_x aggregate is seen in S5c-1, but it transforms into a layer-structure by S5c-8. And even after full removal of Cu₂O, Figure S5d,e, there were changes in the surface morphology of the copper particles. This is typical of reduction processes on metal-oxide interfaces where the generated copper atoms are not in their most stable surface state. 15,23,36,49 These copper atoms probably form part of terraces or steps which are continuously evolving. 15,23,49

In general, we found that the chemical and structural changes seen in **Figures S4** (oxidation) and S5 (reduction) were reversible as seen in XRD (**Figure 1d**), XAS (**Figure S2**) and AP-XPS

(**Figure S6**). A switch of $Cu^0 \leftrightarrow Cu^{+1} \leftrightarrow Cu^{2+}$ oxidation states was relatively easy, there were changes in the structure and location of TiO_x or Cu-Ti- O_x aggregates, and the sample, even after extensive oxidation with O_2 at high temperature, always had some Ti^{3+} cations present (**Figure S2**). The Cu-Ti- O_x mixed-oxide systems are known to exhibit an inherent concentration of Ti^{3+} sites that are very difficult to remove by oxidation. A random distribution of Cu and Ti^{3+} centers is probably responsible for a lack of crystallization of the Cu-Ti- O_x phase. All these properties are a consequence of strong metal-support interactions that are couple to the generation/disappearance of a mixed-metal oxide and can have a positive impact on the reactivity of the system towards CO_2 , 17,22 H_2 , 18,20,21 and the hydrogenation of CO_2 . $^{17-21}$

B. CO₂ hydrogenation: Oscillations in catalytic activity

On the pre-reduced Cu@TiO_x sample, activity measurements were carried out for CO₂ hydrogenation at 250 (**Figures 4**) and 350 °C (**Figure S7**) Under CO₂ hydrogenation conditions, CO was the only reaction product as a consequence of the reverse water-gas shift reaction (rWGS, $CO_2 + H_2 \rightarrow CO + H_2O$). This is expected, since the catalytic measurements were done at atmospheric pressures where no methanol is produced.^{19,20} In the temperature range investigated, 250-350 K, we did not detect the formation of methane or other light hydrocarbons. Thus, the catalytic tests point to a partial decomposition of CO_2 on the catalyst surface. In **Figure 4**, each cycle lasts 5 hours. The catalyst was exposed to the reacting gases at 25 °C and the temperature was raised to 250 °C. The initial activity at 250 °C was large and decreased (by 30-40%) with time. Moreover, when the activity was measured during multiple cycles following the same temperature program of cooling to RT and then heating to 250 °C, a stable pattern eventually was

observed in **Figure 4** after the third cycle (t > 15 hours). A similar behavior was seen when the temperature was set at a final value of 350 °C (**Figure S7**). At both temperatures, the drop in

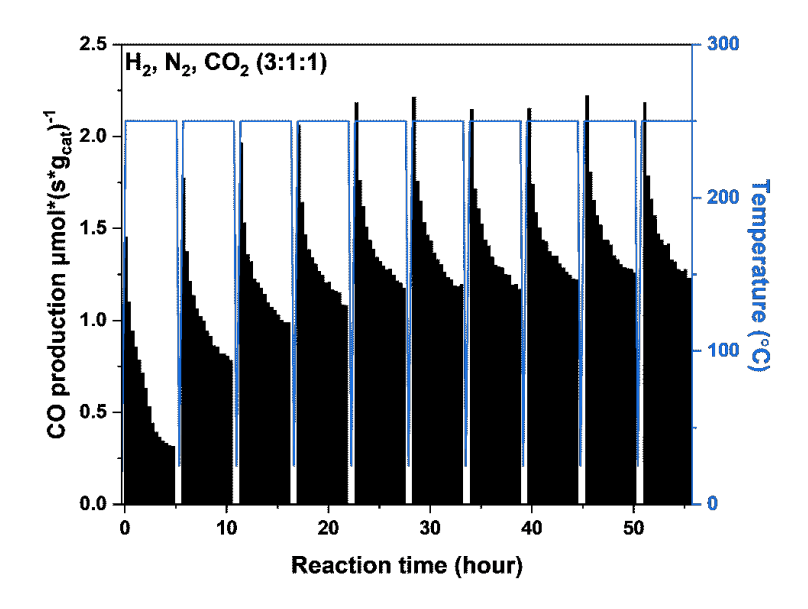


Figure 4. The CO₂ hydrogenation activity was measured on a freshly reduced Cu@TiO_x sample at 250 °C in a continuous experiment, composed of 10 cycles. In each cycle, the temperature is raised from room temperature to 250 °C, then kept at 250 °C for 5 h, and subsequently cooled down to room temperature in a reaction gas mixture of $v(H_2)$: $v(CO_2)$: $v(N_2)$ = 3:1:1.

catalytic activity was substantial, making necessary an analysis of the transient stage to fully understand the behavior of Cu@TiO_x during the catalytic process.

C. CO₂ hydrogenation: Changes in chemical state

In-situ XAS and XRD were used to follow the chemical state of the Cu@TiO_x catalyst under CO₂/H₂ mixtures typically used in the conversion of CO₂ to CO, oxygenates or alkanes. ¹⁸⁻²¹. The TEM and EELS results in **Figures 3** and **S3** point to an active configuration which contains nanoparticles of copper partially covered by aggregates of TiO_x or Cu-Ti-O_x. It is known that, at room temperature (RT), carbon dioxide undergoes partial dissociation (CO₂ \rightarrow CO + O_{oxide}) over Cu(I)/TiO_{2-x} nanoparticles ¹⁷ and over steps and defects of extended surfaces of copper. ^{52,53,54} All

the in-situ techniques used in this work point to the oxidation of copper and TiO_x by CO_2 at RT and reduction of CuO_x and Cu-Ti- O_x by H_2 at 250 0 C. **Figure 5** displays Cu K-edge XAS data collected while the $Cu@TiO_x$ system was exposed to a CO_2/H_2 mixture at different temperatures. Spectra for the Cu K-edge of Cu_2O and CuO are shown in an inset at the bottom right side of the figure. The energy position of the first peak in the range of 8980-8983 eV decreases when going from Cu^{2+} to $Cu^{0.11, 45}$ In **Figure 5**, one can distinguish two types of behavior. From 38 to 113 $^{\circ}$ C, $a \rightarrow b$ spectra, the position of the XAS features indicates that copper is being oxidized by

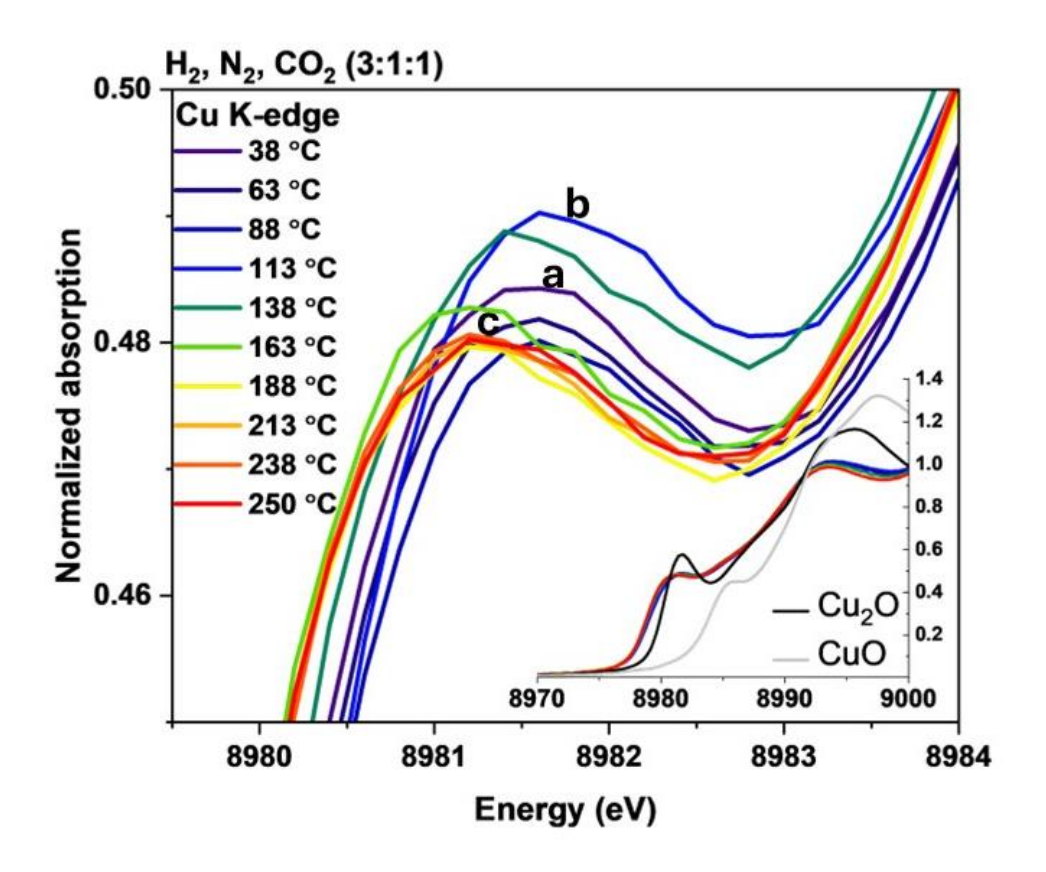


Figure 5. Evolution of the pre-edge feature in *in-situ* XANES Cu K-edge data collected for a Cu@TiO_x catalyst during the ramping from room temperature to 250°C under an H₂, N₂, CO₂ (3:1:1) environment. Inset: The complete *in-situ* XANES data set alongside Cu₂O and CuO standards (the data at 250 °C matches the spectrum for a Cu foil).

 CO_2 decomposition to form CuO_x or Cu-Ti- O_x units. And from 138 to 190 °C, $b \rightarrow c$ spectra, the formed copper cations are being reduced by reaction with H_2 . At 250 °C, the final state essentially contains metallic Cu. The copper particles of reduced $Cu@TiO_x$ contain small clusters of TiO_x on their surfaces (**Figure 3e,f** and **3h,i**). These titania clusters probably help with the dissociation of CO_2 . The dual sites present in a Cu-Ti O_2 interface should facilitate the binding and partial dissociation of CO_2 . At high temperatures (> 140 °C), the oxygen atoms generated by the $CO_{2,gas} \rightarrow CO_{gas} + O_{oxide}$ process are rapidly removed by reaction with hydrogen.

The Ti K-edge XAS spectra for the Cu@TiO_x catalyst under CO₂ hydrogenation conditions (**Figure S8**) were very similar to those found under pure H₂ (**Figure S2**). There were clear differences with respect to the spectra for pure TiO₂ and Ti₂O₃ (**Figure S8a**), and the amount of Ti³⁺ present was relatively small at low and high temperatures (**Figure S8b**).

Figure 6 displays *in-situ* XRD patterns collected after performing several cycles of CO₂ hydrogenation on a Cu@TiO_x catalyst. We will start by analyzing the features in the (b) and (e) panels that correspond to a temperature of 250 °C and are the least complex. Using the standards displayed in Figure 1e, the diffraction peaks in 6b,e can be assigned to TiO₂-anatase and metallic Cu. This agrees with the in-situ XAS data shown in Figures 5 and S8. At 250 °C, under a CO₂/H₂ atmosphere, the Cu@TiO_x catalyst had a composition identical to that found under pure H₂ (Figure 1d). The diffraction patterns shown in Figure 6a were collected while heating the Cu@TiO_x under an atmosphere of CO₂/H₂ from 25 to 250 °C. Extra features appear at 5.5-5.8° in 2θ as consequence of the formation of a copper oxide (Figure 1e). As in the case of the in-situ XANES, data in Figure 5, we could identify two types of behavior. From 15 to 120 °C, the position of the new diffraction features indicates that copper is being oxidized by CO₂ dissociation. And from 140 to 190 °C, the produced CuO_x is being reduced by reaction with H₂. At 250 °C, only the lines for metallic Cu and

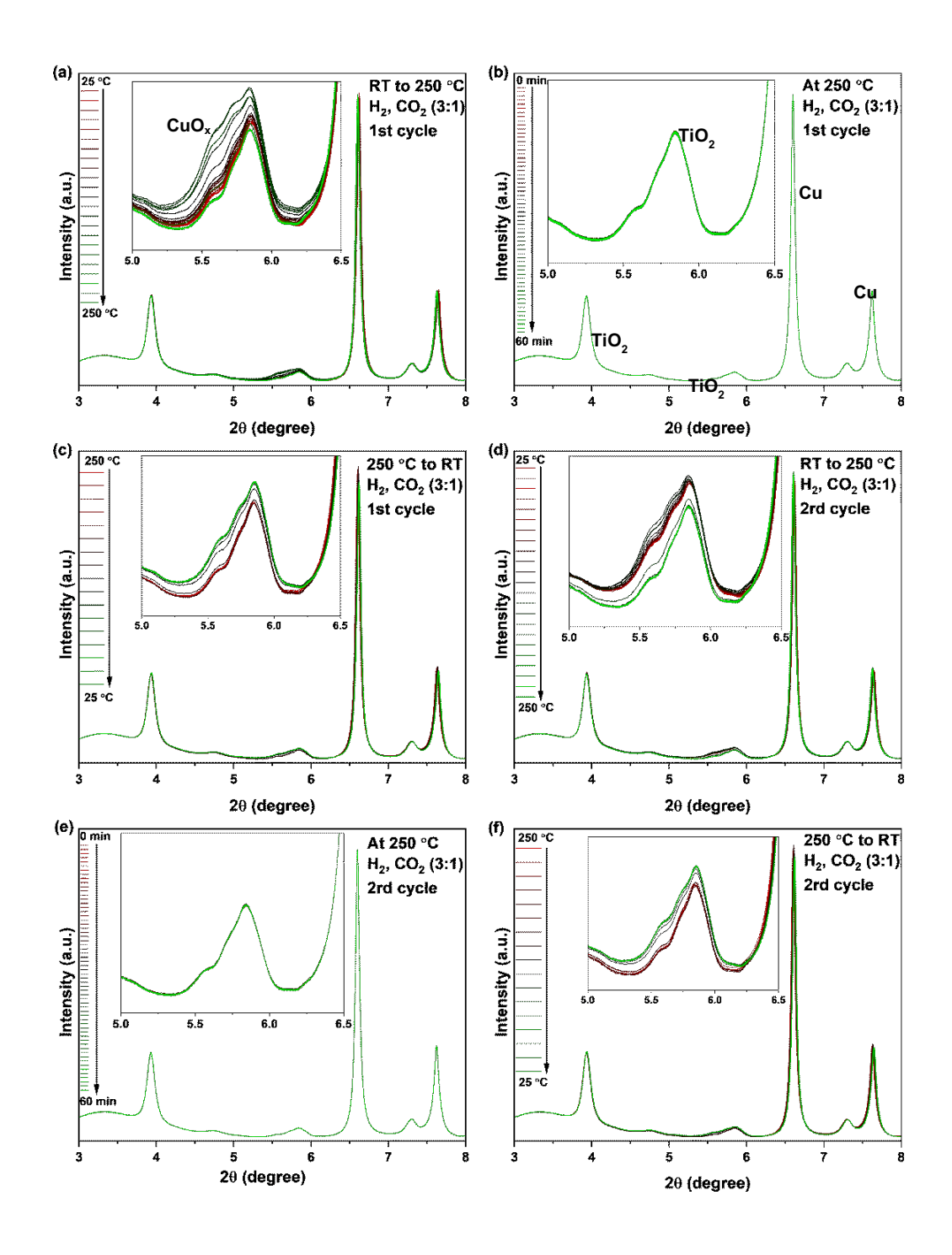


Figure 6. *In-situ* time-resolved XRD data for a $Cu@TiO_x$ catalyst taken under a mixture of $H_2:CO_2$ (3:1) while heating from room temperature (RT) to 250 °C (**a** and **d**), holding at 250 °C (**b**

and **e**), and while cooling from 250 to RT (**c** and **f**). The *in-situ* XRD experiments were carried out using a pre-reduced sample in H_2 at 450 °C.

TiO₂-anatase are seen. This is the starting point for the data sets in panels (c) and (f) where the sample was cooled from 250 to 25 °C under a CO₂/H₂ atmosphere. In these data sets, the diffraction features for CuO_x started to grow at temperatures below 100 °C. From the cycles in **Figure 6**, we can conclude that there are substantial changes in the sample composition at low and high temperatures. The in-situ XANES (**Figure 5**) and XRD (**Figure 6**) data indicate that neither CO₂ (oxidation of the catalyst) nor H₂ (reduction of the catalyst) are passive reactants.

D. CO₂ hydrogenation: Morphological changes

The results of XAS and XRD point to a catalyst composition involving Cu, TiO_2 and Cu-Ti-O_x at the elevated temperatures (> 200 °C) used for the hydrogenation of CO₂. We will start by examining the morphology of this composition. The left-side panel in **Figure 7** shows an image of E-TEM collected for a Cu@TiO_x catalyst under moderate pressures of CO₂ and H₂ at 250 °C. The AP-XPS data in the right-side show that these moderate pressures are enough to reach the

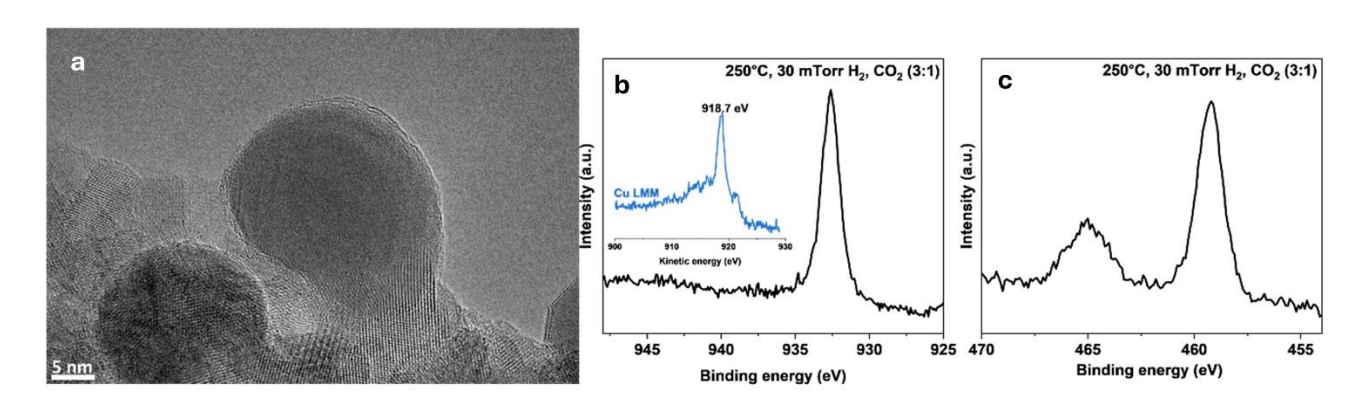


Figure 7. Characterization of a sample focusing on the surface morphology (**a**) and electronic structure (**b-c**) under CO_2+H_2 environments at 250°C. (**a**) E-TEM image of the sample taken under 0.2 mTorr of CO_2 and 9.8 mTorr of H_2 . (**b-c**) AP-XPS of $Cu\ 2p_{3/2}$ (**b**), $Cu\ LMM$ (**b inset**), and $Ti\ 2p\ data$ (**c**) collected under a 30 mTorr H_2+CO_2 (3:1) atmosphere.

final composition found under atmospheric pressures: metallic copper plus TiO_{2-x} or $Cu-Ti-O_x$. The small asymmetry in the Ti 2p indicates that the concentration of Ti^{3+} centers is below 5%. The catalyst composition and morphology under CO_2/H_2 are very similar to those observed under pure H_2 at elevated temperatures (**Figures 1c, 3**, and **S3**).

Following the *in-situ* XAS and XRD studies in **Figures 5** and **6**, which show dissociation of CO₂ at RT, a result consistent with previous studies for Cu and Cu-TiO₂ interfaces, 17,52,53 we investigated with E-TEM the morphological changes that will follow after exposing a Cu@TiO_x system pre-reduced in H₂ (**Figure 3a-f**) to CO₂/H₂ gas mixtures at 20 °C (**Figure 8a,c**). The images of E-TEM showed the growth of an amorphous overlayer, which can be attributed to a mixture of CuO_x/Cu-Ti-O_x, 23,38,39 on top of a dark core of metallic copper. Inside this overlayer small local

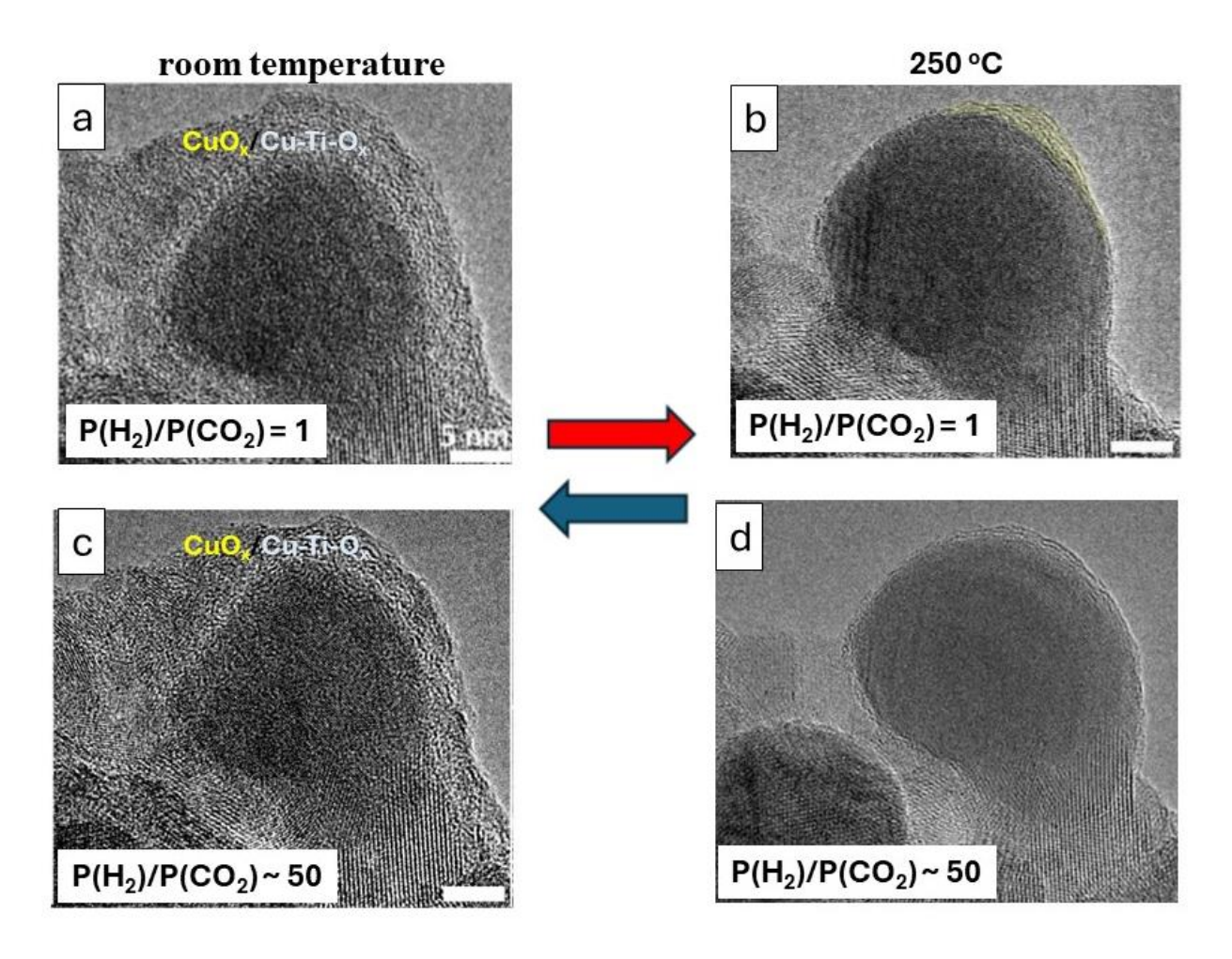


Figure 8. E-TEM images collected while exposing a pre-reduced Cu@TiO_x catalyst to (a,b) 20 mTorr of CO₂ and H₂ { $p(H_2)/p(CO_2)=1$ }, and (c,d) 0.2 m Torr of CO₂ and 9.8 mTorr of H₂ { $p(H_2)/p(CO_2) \sim 50$ }. Images (a) and (c) were recorded at room temperature, while (b) and (d) were collected at 250 °C. The changes in surface composition and morphology were reversible. Scale bar = 5 nm.

fringes of Cu₂O were seen. This growth mode has been observed with TEM for the onset of the oxidation with O₂ of plain metallic copper^{38,39} or pre-reduced Cu@TiO_x (**Figure S4a**). Furthermore, CO₂ can facilitate the formation of two-dimensional amorphous titania. ⁵⁶ The oxide overlayers seen in **Figure 8** did not grow when the pre-reduced sample was manipulated or heated in vacuum (**Figure S9**) and they are not the product of beam damage (**Figure S10**). Co-exposure with molecular H₂ at RT had only a minor effect on the oxide overlayer induced by CO₂ dissociation (**Figure 8a,c**). However, the oxide overlayer did not survive in the presence of hydrogen when the temperature was raised above 200 °C (**Figures 7a** and **8b,d**), in close agreement with the stability seen in XAS (**Figure 5**) and XRD (**Figure 6**) or in the reduction of pure copper oxides. ^{11,45,46}

In experiments of AP-XPS, we did not see deposition of atomic carbon, but some surface carbonate species (CO_x) could be present in the system as a result of the reaction of CO₂ with O centers of titania. ⁵⁷ Also no significant amount of carbon was detected in EELS (**Figure S11**). This is in agreement with experiments of infrared spectroscopy and AP-XPS which indicate that there is only partial decomposition of CO₂ on Cu(I)/TiO_{2-x} nanoparticles¹⁷ and on surfaces of metallic copper. ^{40,41} Furthermore, CO does not dissociate on nanoparticles¹⁷ and surfaces³⁶ containing Cu-Ti-O_x units.

The morphological changes seen in **Figure 8** were completely reversible with temperature, reflecting a balance between the oxidizing power of CO₂ (low temperature) and the reducing power of H₂ (high temperature). Furthermore, even when the ratio of H₂/CO₂ was increased by a factor

of 50, the switch in the catalyst morphology was observed after cooling the sample to room temperature (**Figure 8c**). As seen in the experiments of XAS and XRD, neither CO₂ (oxidation of the catalyst) nor H₂ (reduction of the catalyst) can be classified as passive reactants.

The experimental conditions used in the experiments of **Figures 4** (catalytic tests), **5** (XANES), and **6** (XRD) are similar. The E-TEM experiments in **Figures 7** and **8** were conducted under moderate pressures, but the final composition of the catalyst was identical to that found in *in-situ* studies with XAS (**Figure 5**) and XRD (**Figure 6**) at atmospheric pressures. Furthermore, the final morphology under steady state seen in **Figure 7a** matches well that found in a *post-mortem* analysis (**Figure 9**) for Cu@TiO_x after performing the atmospheric experiments of **Figure 4**. The Cu@TiO_x catalyst had a large reactivity and the material evolved to the same chemical composition at 250 °C.

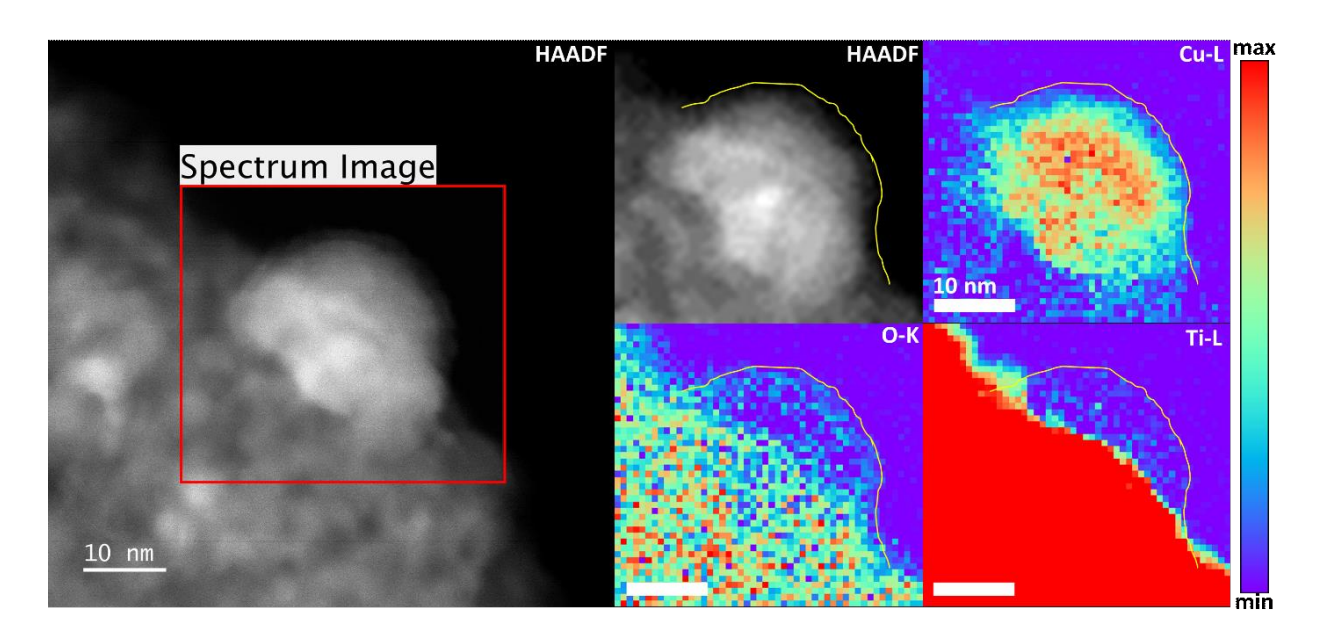


Figure 9 High-angle annular dark field (HAADF) images of lower magnification and the selected area, as well as its energy-dispersive X-ray spectroscopy (EELS) mapping on Cu L-edges, O K-edge, and Ti L-edges of a post-reaction sample after CO₂ hydrogenation reaction in a reactor at 1 atm. The yellow line in the EELS mapping serves as a reference for better identifying the corresponding regions.

From the XAS (**Figure 5**), XRD (**Figure 6**), AP-XPS (**Figure 7b,c**) and TEM (**Figures 7a** and **8**) studies, it is clear that the active catalysts in **Figure 4** contained a mixture of Cu, TiO_x and Cu-Ti-O_x. The exact morphology of the catalyst surface is probably changing and affected by the fact that the system was cooled to room temperature where CO₂ can oxidize the sample. The Cu-TiO₂ interface favors the dissociation of CO₂, ^{17,22} and the generated CuO_x/Cu-Ti-O_x oxide is highly effective for the splitting of H₂, ^{21,23} but it does not survive under hydrogen rich atmospheres at high temperatures (> 180 °C). **Figure 10** summarizes the major changes in chemical state seen for the Cu@TiO_x catalyst. The peaks in catalytic activity in **Figure 4** are probably associated with a surface, produced by the reduction process, that is metastable and rich in atoms with a low coordination number. ^{15,23,36,46} In this surface, the Cu atoms and TiO_x aggregates are

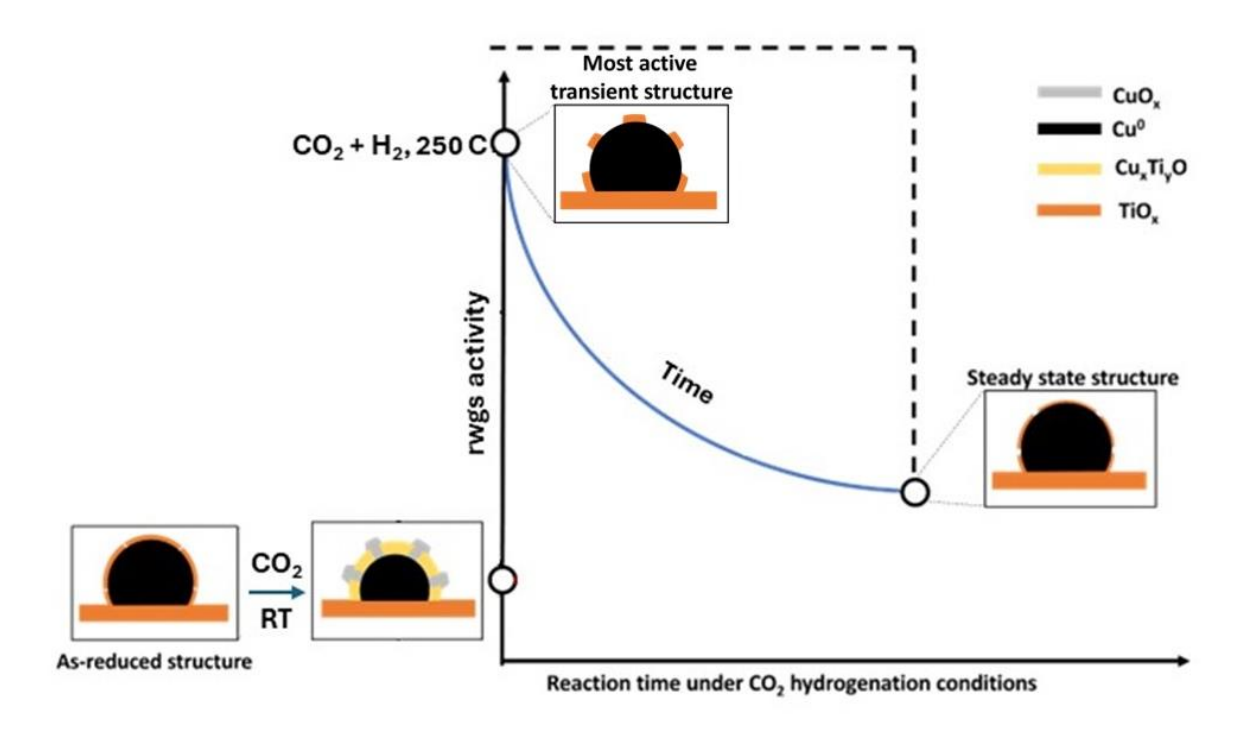


Figure 10. Main changes in chemical state of the $Cu@TiO_x$ catalyst under different reaction conditions. Neither CO_2 nor H_2 are passive reactants. The catalytically active CuO_x/Cu_xTi_yO surface formed by reaction with CO_2 at 25 °C (**Figure 8a,c**) is not stable at elevated temperatures under an H_2 atmosphere (**Figures 7** and **8b,d**). Under steady-state, the catalyst adopts an inverse oxide/metal configuration with particles of Cu partially covered with TiO_x or Cu-Ti- O_x . The

configuration of the surface copper atoms and $TiO_x/Cu-Ti-O_x$ aggregates changes during the reduction process. Metastable sites with a low coordination number are initially generated during reduction that disappear as time progresses (**Figures 3, S5** and **8**).

probably moving on unstable terraces or steps, as seen in STM and TEM studies for the reduction of copper oxides and Cu-Ti-O_x, ^{15,23,46,49} and they lose chemical and catalytic activity when reaching their equilibrium configuration in the final steady-state. ^{17,23,53,58} Evidence was found for a redistribution of Cu and TiO_x aggregates on the catalysts surface during the oxidation/reduction process (**Figures 3**, **S3**, **S5 and 8**) that certainly can affect the overall activity of the system. A similar phenomenon was observed in a Cu-Ti-O_x catalyst active for H₂-D₂ exchange. ²³ Thus, the active phase of the catalyst involved a dynamic inverse oxide/metal configuration, i.e. particles of copper covered by aggregates of TiO_x or Cu-Ti-O_x, where the composition, structure and reactivity of the system were very sensible to the temperature and reactants in CO₂ hydrogenation. The nature and concentration of the active sites were very sensitive to the chemical environment and temperature around the catalyst (**Figures 3, 8, S4** and **S5**). A full understanding of this type of catalyst cannot be extracted from conventional steady state experiments.

E. Metal-support interactions: Reversible chemical and morphological changes during the binding and hydrogenation of CO₂

Our studies indicate that metal-support interactions had a strong impact on the structural properties of Cu@TiO₂ catalysts. On purpose, following previous works for core-shell nanostructured catalysts,^{34,59} we started with a Cu@TiO₂ configuration¹⁹ that mimicked the inverse oxide/metal configuration seen for several CO₂ hydrogenation catalysts.^{8-11,60} However, this pristine core@shell configuration was not stable under H₂ or CO₂/H₂ mixtures. The oxide shell cracked and copper was present in three regions of the catalyst: (i) as a nanowire encapsulated by

a TiO_2 shell, (ii) as a component in a Cu-Ti- O_x mixed oxide, and (iii) as metal particles on top of the oxide shell that were decorated by TiO_x clusters. These copper-titania interfaces are important because they are directly involved in the activation of CO_2 and H_2 in catalysts for CO_2 hydrogenation. 17,21,22

Since the surface of the catalyst responded to the presence of CO₂ and H₂, morphological changes were observed during CO₂ hydrogenation that have not been detected previously in E-TEM images collected while exposing metal/oxide catalysts to either plain H₂ or CO oxidation conditions. ^{29,61,62} These morphological changes may be responsible for the difficulties reported when establishing the active phase for catalysts used in CO₂ hydrogenation. ^{7-11,13,14,16,63} The E-TEM results in **Figures 3, 7, 8, S4** and **S5** showed that the surface morphology of the Cu@TiO_x catalyst was far from being static and evolved with changes in the chemical environment and temperature. The inverse oxide/metal configuration was a dynamic entity with the distribution of TiO_x aggregates on top of the copper particles changing in different ways in the presence of H₂, O₂ or CO₂. Reaction with O₂ and CO₂ led to oxidation of the copper component with the formation of amorphous structures which had small fringes of Cu₂O or CuO. These oxide overlayers had a high reactivity toward H₂ and could be removed by reduction at 150-180 °C.

In the case of $ZnO/CuO_x/Cu(111)$ surfaces, the supported ZnO nanoparticles dissociate H_2 molecules and the produced H atoms accelerate the reduction of the copper oxide in the sample inducing morphological changes not seen for plain $CuO_x/Cu(111)$. A similar phenomenon could be occurring on the $Cu@TiO_x$ and $Cu/ZnO/Al_2O_3$ catalysts. The inverse oxide/metal configuration can exploit the fact that ZnO and TiO_x clusters can readily dissociate the H_2 molecule. 15,21,64,65,66 Indeed, for the $Cu/ZnO/Al_2O_3$ and $Cu@TiO_x$ catalysts, the structural and morphological changes

associated with the reduction of the copper oxide component in H_2 or CO_2/H_2 show clear differences with respect to those seen in plain copper oxide systems with E-TEM.^{46,47}

Adsorbate-induced metal-support interactions have been the focus of many studies in recent years. ^{23-27,29} Hydrogen is the typical adsorbate that drives the catalyst surface reconstruction, ^{9,10,23-27,29,67} but the phenomenon also has been observed with other adsorbates (CO, HCO_x x= 2 or 3). ^{11,25-28,58,68,69,70} This is the first time that pure CO₂-induced morphological changes associated with the formation of an oxide (CuO_x and Cu-Ti-O_y for the system under study here) are reported. In recent E-TEM studies for Cu/ZnO/Al₂O₃ catalysts only exposures to pure H₂ or CO₂/H₂ mixtures were investigated, ^{9,10} and it is not known how the morphology of the ZnO/Cu interfaces can change in the presence of CO₂ as a function of temperature. Due to the high stability of its C-O bonds and its non-polar nature, the activation of CO₂ is not an easy task. In general, it is difficult to bind the CO₂ molecule well. ^{4,5,71} However, the formation of a metal-oxide interface can produce compounds that bind and activate CO₂ at room temperature. ^{17,72} From our results, it is clear that when dealing with a system that is efficient for the binding and conversion of CO₂, one must consider the effects of the molecule on the surface morphology of the system.

When comparing our E-TEM results with those reported for the hydrogenation of CO_2 to methane on TiO_2/Ni , 30 one sees clear differences in the behavior of these metal-oxide interfaces. In both systems, metal-support interactions induce the migration of TiO_x clusters or aggregates that land on top of the metal component (Cu or Ni), but in the catalyst for CO_2 methanation, carbon plays a clear role when determining the structure and morphology of the surface 30 that is not seen in the case of $Cu@TiO_x$, where the interactions with CO_2 and CO_2/H_2 mixtures are reversible.

Neither Cu nor Cu-TiO_x interfaces fully dissociate the CO₂ molecule and methane was not a product seen on the Cu@TiO_x catalyst.

In recent works, it has been proposed that metal-support interactions can be useful when enhancing the dispersion of metals in heterogeneous catalysts. ²⁵⁻²⁷ It is certainly a valid approach, but our study shows a series of phenomena that must be taken into consideration when following this path. In a metal-oxide interface both components can underdo dramatic changes in composition and structure that are very difficult to predict as a function of gas composition and temperature. The Cu@TiO_x catalyst adopted an inverse oxide/metal configuration under reaction conditions that was very dynamic and different from the initial core@shell structure.

Conclusion

In-situ characterization methods highlight dynamic changes in the composition and structural properties of a Cu@TiO_x core@shell system under O_2 , H_2 , CO_2 and CO_2 hydrogenation conditions. Metal-support interactions coupled with the formation of a mixed-metal oxide changed the catalyst configuration and produced new copper-titania interfaces with high chemical activity. Pre-treatment in O_2/H_2 disrupted the initial core@ shell configuration with the titania shell cracking and Cu particles migrating from the core to on top of the oxide. The generated Cu particles had a diameter of 20-40 nm and were partially decorated by small (< 5 nm in size) aggregates of TiO_x or Cu-Ti- O_x . At room temperature, CO_2 was very reactive on this inverse oxide/metal interface, oxidizing ($CO_2 \rightarrow CO + O_{oxide}$) the copper component to yield CuO_x and Cu-Ti- O_x units, and producing big changes in the catalyst surface morphology. The Cu-Ti- O_x generated by the partial dissociation of CO_2 was not stable at elevated temperatures (> 200 $^{\rm o}C$) in the presence of H_2 .

In-situ XAS, XRD, AP-XPS and E-TEM studies performed under CO₂/H₂ mixtures indicated that the Cu@TiO_x catalyst gradually evolved towards a dynamic equilibrium structure

that was temperature dependent. Cu was always at the core but, on top of the metal, the distribution of TiO_x and Cu-Ti- O_x aggregates depended on the history of the system. This study underscores the dynamic nature of the surface in the $Cu@TiO_x$ catalyst. Changes detected in the presence of CO_2 and CO_2/H_2 mixtures were reversible. This is a very important property to establish an effective catalytic cycle, since CO_2 and H_2 were not passive reactants and both modified the morphology of the catalyst. When dealing with CO_2 activation or hydrogenation, fundamental insights can be obtained from transient studies, because a full but absolutely necessary understanding of the prevailing structure under operating conditions cannot be extracted from either ex situ images or conventional steady state research.

Materials and Methods

Catalyst preparation. The initial samples consisted of Cu@TiO₂ core@shell nanowires, generated using a methodology described in detail in a recently published paper by our group.¹⁹ It involved a micro-wave assisted method where the molar ratio of copper or titanium cations in the chemical precursors was carefully controlled.¹⁹ In a first step, Cu nanowires were prepared using a CuCl₂·2H₂O chemical precursor. After a hydrothermal synthesis, they exhibited the fcc phase (JCPDS #03-1018) of pure copper, as corroborated by XRD results.¹⁹ In a second step, a TiO₂ shell was added to the Cu nanowires using TBOT as a chemical precursor.¹⁹ The fresh Cu@TiO₂ showed a core-shell structure in TEM (**Figure 1a** and ref 19). In XAS and XPS, the main species detected were Ti⁴⁺ and Cu⁰ plus copper partially oxidized (Cu^{δ+}) at the metal-oxide interface.¹⁹ The assynthesized core@shell nanowires were treated in a reactor with 1 bar pressure with the following sequence: 1 h in 10 v% O₂ at 350 °C and then 1 h in 50 v% H₂ at 450 °C with a 10 °C/min ramping

rate for heating and a 15 °C/min ramping rate for cooling. After treatment, the sample is referred to as "pre-reduced" throughout this paper.

Catalytic activity measurements. The catalytic performance of the materials was evaluated in a continuous-flow, fixed-bed microreactor at about 1 atm pressure. Around 1.2 mg of the Cu/TiO_x sample were loaded in a quartz capillary of 1.1 mm OD and 0.9 mm ID. Before activity measurements, and after treatment in O_2 , the sample was reduced at 450 °C under 50 v% H_2/N_2 (see above). For activity measurements at 350 °C, a total flow of 12 standard cubic centimeters per minute (sccm) was used, while a 2.5 sccm flow was utilized for measurements at a 250 °C reaction temperature. The composition of the gas mixture evolved from the reactor was analyzed using a gas chromatograph (Agilent 7890A), equipped with both flame ionization and thermal conductivity detectors. The N_2 in the gas flow was used as the internal standard. The only product observed during CO_2 hydrogenation was CO. No methanol or methane were detected.

X-ray diffraction (XRD). The data were collected in the 17-BM-B beamline at the Advanced Photon Source (APS) in Argonne National Laboratory (ANL) using an area detector with an X-ray wavelength of 0.24012Å. The sample was loaded in a Clausen cell (0.9 mm ID and 1.1 mm OD quartz capillary) and the whole experiment was carried out under in-situ conditions reproducing the conditions used in the catalytic tests for CO₂ hydrogenation at 250 °C (see above). Rietveld refinements⁷³ were conducted in the data analysis with the GSAS-II code,⁷⁴ using the known diffraction patterns for metallic Cu, Cu₂O, CuO, TiO₂ anatase and CuTiO₃ as references (**Figure 1e** and ref. 31).

X-ray Absorption Spectroscopy (XAS). Most of the in-situ X-ray absorption fine structure (XAFS) spectra were collected at the 7-BM Quick x-ray Absorption Scattering (QAS) beamline

of the National Synchrotron Light Source II (NSLS-II) at Brookhaven National Laboratory (BNL). Some of the XAFS traces were collected at the 8-ID Inner-Shell Spectroscopy (ISS) beamline of NSLS-II at BNL. In these characterization studies, powder samples were drop-casted onto aluminum foil and both the Cu K edge and Ti K edge spectra were collected in the transmission mode with the photon energies calibrated with Cu and Ti foil as standards, respectively. A Nashner-Adler cell ⁷⁵ was used for the *in-situ* measurements following the working procedure employed for the catalytic tests (see above). The XAFS spectra were analyzed using the Athena software. ⁷⁶ A k range of 2-12 Å⁻¹ was used for the Fourier transform of the Extended X-ray absorption fine structure (EXAFS) data. The analysis of the Cu K-edge spectra was done using metallic Cu, Cu₂O and CuO as reference compounds (inset in **Figure 5**). The corresponding spectra for Ti₂O₃ and three phases of TiO₂ (rutile, anatase and brookite) were used in the analysis of the Ti K-edge spectra (**Figures S2** and **S8**).

Ambient Pressure X-ray Photoelectron Spectroscopy (AP-XPS). The ambient pressure X-ray photoelectron spectroscopy (AP-XPS) spectra displayed in Figure 2 were collected at the 23-ID-2 beamline of the National Synchrotron Light Source II at BNL. The standard Cu 2p3/2 binding energy (932.6 eV) was used for energy calibration. A lab-based AP-XPS was used to collect the data displayed in Figure 7 and S3. It consists of a SPECS AP-XPS chamber, equipped with a PHOIBOS 150 EP MCD-9 analyzer with an energy resolution of 0.4 eV. The Cu²⁺ was calibrated to 933.6 eV, and then Cu⁺ was used for Cu⁰ alignment.

Scanning transmission electron microscopy (STEM). The FEI Talos F200X at the Center for Functional Nanomaterials (CFN) of BNL was used to collect high-angle annular dark-field (HAADF) STEM data, energy-dispersive X-ray spectroscopy (EDS) data.

Electron Energy Loss Spectroscopy (EELS). The Hitachi 2700C at the CFN in BNL was used to collect EELS data as well as ex situ TEM data in **Figure 11** and **S10** at an accelerating voltage of 200 kV. The instrument has a probe aberration-corrector to achieve high imaging spatial resolution. The EELS data were processed using hyperspy/(hyperspy: Release v1.7.3.⁷⁷

Environmental transmission electron microscopy (E-S/TEM). The E-TEM images as well as the E-STEM-ADF and E-STEM-EELS data were collected at the CFN in BNL using an FEI Titan 80-300 equipped with an objective-lens aberration corrector and operated at an accelerating voltage of 300 kV. The *in-situ* TEM sample was prepared by drop-casting a suspension of pre-reduced Cu/TiO_x in water onto a MEMS-based heating chip (through-hole chip of DENSsolutions Wildfire series).

All the E-TEM experiments were performed using Cu@TiO_x samples that were prereduced in H₂ outside the microscope as done for the catalytic tests (see above). Inside the
microscope, the samples were again reduced in H₂ before exposing them to CO₂ or CO₂/H₂
mixtures. Since the E-TEM instrument was properly cleaned, the morphological changes seen
upon exposure to O₂ and CO₂ (associated with dissociation of these molecules and the formation
of oxide overlayers) were not observed when the samples were heated inside the TEM without
O₂ or CO₂ in the background. These morphological changes match those reported in the
literature for TEM studies for the oxidation of metallic copper or Cu-Ti-O_x. ^{23,38,39} In addition,
some regions in the samples were briefly examined with e-beam exposure times of less than 1
minute to assess the impact of e-beam irradiation on the sample's structure. The observed
structure appeared comparable with and without an extended period of e-beam irradiation,
indicating that the effect of e-beam irradiation on the image structures can be ruled out.
Experiments were done with H₂/CO₂ pressure ratios that varied from 1 to 50. At a temperature

of 250 °C, changing of the H₂/CO₂ reactant ratio from 1 to 50 did not affect the final composition of the catalytic surface.

Data availability

The data that support the findings of this study are presented in the article and Supplementary Information. Source data are provided with this paper. Any other relevant data are also available from the corresponding author (J.A. Rodriguez) upon reasonable request.

Competing interests

The authors declare no competing interests.

Associate Content

Supporting Information

The Supporting Information is available free of charge at

Additional details for characterization studies with E-TEM, STEM, EELS, XRD, XAS and XPS.

Acknowledgement

The work done at the Chemistry Division of BNL was supported by the U.S. Department of Energy, Office of Science, Office of Basic Energy Sciences, and Catalysis Science Program under contract No. DE-SC0012704. J.A.R. and J.M. received funding from a DOE Office of Science Distinguished Scientist Fellow Award. X.C. and G.Z acknowledge the support by the National Science Foundation (NSF) under DMR 1905422. A.I.F. acknowledges support of XAFS data

analysis by the U. S. DOE, Office of Science, Office of Basic Energy Sciences grant no. DE-SC0022199. The Cu@TiO_x core-shell nanowires, that inspired the current work, were initially produced in SSW's laboratory, supported by the U.S. National Science Foundation under Grant No. CHE-1807640. This research used resources of beamlines 7-BM (QAS), 28-ID-2 (XPD), and 23-ID-2 (IOS) of the National Synchrotron Light Source II, a U.S. Department of Energy (DOE) Office of Science User Facility operated for the DOE Office of Science by Brookhaven National Laboratory under Contract No. DE-SC0012704. The QAS beamline operations were supported in part by the Synchrotron Catalysis Consortium (U.S. DOE, Office of Basic Energy Sciences, Grant No. DE-SC0012335). This research used resources of beamline 17-BM at the Advanced Photon Source, a U.S. Department of Energy (DOE) Office of Science user facility operated for the DOE Office of Science by Argonne National Laboratory under Contract No. DE-AC02-06CH11357. The morphology of the catalyst was studied at the Electron Microscopy Facility (FEI Titan 80-300 and FEI Talos 200x) of the Center for Functional Nanomaterials (CFN), which is a U.S. Department of Energy Office of Science User Facility, at Brookhaven National Laboratory under Contract No. DE-SC0012704. The authors are grateful to D. Zakharov for his help with some of the E-TEM and EELS studies.

References

¹ Jones, W. D. Carbon Capture and Conversion. J. Am. Chem. Soc. **2020**, 142, 4955–4957.

² Tackett, B. M.; Gomez, E.; Chen, J. G. Net Reduction of CO₂ via Its Thermocatalytic and Electrocatalytic Transformation Reactions in Standard and Hybrid Processes. *Nat. Catal.* **2019**, *2*, 381–386.

³ Anderson, T. R.; Hawkins, E.; Jones, P. D., CO₂, the Greenhouse Effect and Global Warming: from the Pioneering Work of Arrhenius and Callendar to Today's Earth System Models. *Endeavour* **2016**, *40*, 178-187

⁴ Bushuyev, O. S.; De Luna, P.; Dinh, C. T.; Tao, L.; Saur, G.; van de Lagemaat, J.; Kelley, S. O.; Sargent, E. H. What Should We Make with CO₂ and How Can We Make It? *Joule* **2018**, *2*, 825–832.

- ⁶ Omodolor, I. S.; Otor, H. O.; Andonegui, J. A.; Allen, B. J.; Alba-Rubio, A. C. Dual-Function Materials for CO₂ Capture and Conversion: A Review. *Ind. & Eng. Chem. Research* **2020**, *59*, 17612-17631.
- ⁷ Kattel, S.; Ramírez, P. J.; Chen, J. G.; Rodriguez, J. A.; Liu, P. Active Sites for CO₂ Hydrogenation to Methanol on Cu/ZnO Catalysts. *Science* **2017**, *355*, 1296–1299.
- ⁸ Wu, C.; Lin, L.; Liu, J.; Zhang, J.; Zhang, F.; Zhou, T.; Rui, N.; Yao, S.; Deng, Y.; Yang, F.; Xu, W.; Luo, J.; Zhao, Y.; Yan, B.; Wen, X.-D.; Rodriguez, J.A.; Ma, D. Inverse ZrO₂/Cu as a highly efficient methanol synthesis catalyst from CO₂ hydrogenation. *Nat. Commun.* **2020**, *11*, 5767.
- ⁹ Lunkenbein, T.; Schumann, J.; Behrens, M.; Schlögl, R.; Willinger, M. G. Formation of a ZnO Overlayer in Industrial Cu/ZnO/Al₂O₃ Catalysts Induced by Strong Metal-Support Interactions. *Angew. Chem. Int. Ed.* **2015**, *54*, 4544-4548.
- ¹⁰ Huang, X.; Beck, A.; Fedorov, A.; Frey, H.; Zhang, B.; Klötzer, B.; van Bokhoven, J. A.; Copéret, C.; Willinger, M.-G. Visualizing Structural and Chemical Transformations of an Industrial Cu/ZnO/Al₂O₃ Pre-catalyst during Activation and CO₂ Reduction. *ChemCatChem* **2022**, *14*, e202201280.
- ¹¹ Moncada, J.; Chen, X.; Deng, K.; Wang, Y.; Xu, W.; Marinkovic, N.; Zhou, G.; Martínez-Arias, A.; Rodriguez, J.A. Structural and Chemical Evolution of an Inverse CeO_x/Cu Catalyst under CO₂ Hydrogenation: Tuning Oxide Morphology to Improve Activity and Selectivity, *ACS Catal.* **2023**, *13*, 15248–15258.
- ¹² Fernández Villanueva, E.; Lustemberg, P.G.; Zhao, M.; Soriano Rodriguez, J.; Concepción, P.; Ganduglia Pirovano, M.V. Water and Cu⁺ Synergy in Selective CO₂ Hydrogenation to Methanol over Cu/MgO Catalysts, *J. Am. Chem. Soc.* **2024**, *146*, 2024-2032.
- ¹³ Beck, A.; Newton, M.A.; van der Water, L.G.A.; van Bokhoven, J.A. The Enigma of Methanol Synthesis by Cu/ZnO/Al₂O₃-Based Catalysts, *Chem. Reviews*, **2024**, *124*, 4543-4678.
- 14 Mahapatra, M.; Kang, J.; Ramírez, P. J.; Hamlyn, R.; Rui, N.; Liu, Z.; Orozco, I.; Senanayake, S. D.; Rodriguez, J. A., Growth, Structure, and Catalytic Properties of ZnO_x Grown on CuO_x/Cu(111) Surfaces. *J. Phys. Chem. C* **2018**, *122*, 26554-26562.
- ¹⁵ Mehar, V.; Huang, E.; Shi, R.; Rosales, R.; Waluyo, I.; Hunt, A.; Liu, P.; Rodriguez, J.A, Microscopic Investigation of H₂ Reduced CuO_x/Cu(100) and ZnO/CuO_x/Cu(111) Inverse Catalysts: STM, AP-XPS, and DFT Studies, *ACS Catal.* **2023**, *13*, 9857-9870.

⁵ Aresta, M. Carbon Dioxide as Chemical Feedstock; Wiley-VCH, New York, 2010

¹⁶ Shaaban, E.; Li, G. Probing Active Sites for Carbon Oxides Hydrogenation on Cu/TiO₂ using Infrared Spectroscopy, *Communications Chem.* **2022**, *5*, 32.

- ¹⁷ Liu, L., Zhao, C. & Li, Y. Spontaneous Dissociation of CO₂ to CO on Defective Surface of Cu(I)/TiO_{2-x} Nanoparticles at room temperature. *J. Phys. Chem. C* **2012**, *116*, 7904–7912.
- ¹⁸ Pandey, P.H.; Pawar, H.S. Cu Dispersed TiO₂ Catalyst for Direct Hydrogenation of Carbon Dioxide into Formic Acid, *J. CO₂ Utilization*, **2020**, *41*, 101267.
- ¹⁹ Salvatore, K.L.; Deng, K.; Yue, S.; McGuire, S.C.; Rodriguez, J.A.; Wong, S.S. Optimized Microwave-based Synthesis of Thermally Stable Inverse Catalytic Core-shell Motifs for CO₂ Hydrogenation, *ACS Appl. Mater. Interfaces*, **2020**, *12*, 32591-32603.
- ²⁰ Chen, H.; Li, S.; Ma, P.; Chang, K.; Zhao, Z.; Lai, Y.; Zheng, K.; Kuang, Q.; Xie, Z., Lattice-Confined Cu-TiO₂ Catalysts with Significant Improved Activity and Thermal Stability for CO₂ Hydrogenation, *ACS Sustainable Chem. Eng.* **2023**, *11*, 18112-18122.
- ²¹ Pandey, P.H.; Pawar, H.S. Cu Dispersed TiO₂ Catalyst for Direct Hydrogenation of Carbon Dioxide into Formic Acid, *J. of CO₂ Utilization*, **2020**, *41*, 101267.
- ²² Barlocco, I.; Maleki, F.; Pacchioni, G. CO₂ Activation on Cu/TiO₂ Nanostructures: Importance of Dual Binding Site, *Chem. Eur. J.* **2023**, *29*, e202300757.
- ²³ Foucher, A.C.; Lee, J.D.; Qi, Z.; Li, G.; Ouyang, G.; Cui, J.; Boscoboinik, J.A.; Friend, C.M.; Biener, J.; Stach, E.A. Boosting the H₂–D₂ Exchange Activity of Dilute Nanoporous Ti–Cu Catalysts through Oxidation–Reduction Cycle–Induced Restructuring, *Adv. Eng. Mater.* **2023**, *25*, 2201724
- ²⁴ Tauster, S., Fung, S. & Garten, R. L. Strong Metal-Support Interactions. Group 8 Noble Metals Supported on Titanium Dioxide. *J. Am. Chem. Soc.* **1978**, *100*, 170-175.
- ²⁵ Wang, H.; Gao, Z.; Sun, B.; Mu, S.; Dang, F.; Guo, X.; Ma, D.; Shi, C. Engineering Metal-support Interaction to Construct Catalytic Interfaces and Redisperse Metal Nanoparticles, *Chem. Catal.* **2023**, *3*, 100768.
- ²⁶ Li, Y.; Zhang, Y.; Qian, K.; Huang, W. Metal-Support Interactions in Metal/Oxide Catalysts and Oxide-Metal Interactions in Oxide/Metal Inverse Catalysts, *ACS Catal.* **2022**, *12*, 1268-1287.
- ²⁷ van Deelen, T. W.; Hernández Mejía, C.; de Jong, K. P. Control of metal-support interactions in heterogeneous catalysts to enhance activity and selectivity. *Nature Catalysis* **2019**, *2*, 955-970.
- ²⁸ Bruix, A.; Rodriguez, J.A.; Ramirez, P.J.; Senanayake, S.D.; Evans, J.; Park, J.B.; Stacchiola, D.; Liu, P.; Hrbek, J.; Illas, F. A New Type of Strong Metal—Support Interaction and the Production of H₂ through the Transformation of Water on Pt/CeO₂(111) and Pt/CeO_x/TiO₂(110) Catalysts, *J. Am. Chem. Soc.* **2012**, *134*, 8968-8974.

²⁹ Beck, A.; Huang, X.; Artiglia, L.; Zabilskiy, M.; Wang, X.; Rzepka, P.; Palagin, D.; Willinger, M.-G.; van Bokhoven, J. A. The dynamics of overlayer formation on catalyst nanoparticles and strong metal-support interaction. *Nat. Commun.* **2020**, *11* (1), 3220.

- ³⁰ Monai, M.; Jenkinson, K.; Melcherts, A.E.M.; Louwen, J.N.; Irmak, E.A.; Van Aert, S.; Altantzis, T.; Vogt, C.; Van der Stam, W. et al. Restructuring of titanium oxide overlayers over nickel nanoparticles during catalysis. *Science*, **2023**, *380*, 644-651.
- ³¹ Sanakousar, F.M.; Vidyasagar, C.C.; Shikandar, D.B.; Mounesh, Viswanatha, C.C.; Swapna S. Chigari, Electrocatalytic and photocatalytic activity of CuTiO₃ perovskites for complete degradation of methylene blue under sunlight irradiation, *Reaction Chemitry & Engineering*, **2024**,*9*, 388-409.
- ³² Anderson, J. B. F.; Burch, R.; Cairns, J. A. The reversibility of strong metal-support interactions. A comparison of Pt/TiO₂ and Rh/TiO₂ catalysts. *Applied Catalysis* **1986**, 26, 173-180.
- ³³ Seriani, N.; Mittendorfer, F. Platinum-group and Noble Metals under Oxidizing Conditions. *J. Phys.: Condensed Matter* **2008**, *20*, 184023.
- ³⁴ Zhang, Q.; Lee, I.; Joo, J.B.; Zaera, F.; Yin, Y. Core-Shell Nanostructured Catalysts, *Acc. Chem. Res.*, **2013**, *46*, 1816-1824.
- ³⁵ Eshed, M.; Irzh, A.; Gedanken, A. Reduction of Titanium Dioxide to Metallic Titanium Conducted under Autogenic Pressure of the Reactants, *Inorg. Chem.* **2009**, *48*, 7066-7069.
- ³⁶ Baber, A. E.; Yang, X.; Kim, H.Y.; Mudiyanselage, K.; Soldemo, M.; Weissenrieder, J.; Senanayake, S.D.; Al-Mahboob, A.; Sadowski, J.T.; Evans, J. et al. Stabilization of Catalytically Active Cu⁺ Surface Sites on Titanium–Copper Mixed-Oxide Films. *Angew. Chem. In. Ed.* **2014**, *53*, 5336-5340.
- ³⁷ Biesinger, M.C. Advanced Analysis of Copper X-ray Photoelectron Spectra, *Surf. Interface Anal.* **2017**, *49* (8), 1325-1334.
- ³⁸ Košiček, M.; Zavašnik, J.; Baranov, O.; Batič, B.S.; Cvelbar, U. Understanding the Growth of Copper Oxide Nanowires and Layers by Thermal Oxidation over a Broad Temperature Range at Atmospheric Pressure, *Cryst. Growth Des.* **2022**, *22*, 6656–6666.
- ³⁹ Moise, C.C.; Enache, L.-B.; Anăstăsoaie, V.; Lazăr, O.A.; Mihai, G.V.; Rosoiu, S.P.; Bercu, M.; Enăchescu, M. On the Growth of Copper Oxide Nanowires by Thermal Oxidation near the Threshold Temperature at Atmospheric Pressure, *J. Alloys and Compounds*, **2021**, *886*, 161130.
- ⁴⁰ Wu, Z.Y.; Ouvard, G.; Gressier, P.; Natoli, C.R. Ti and O K Edges for Titanium Oxides by Multiple Scattering Calculations: Comparison to XAS and EELS Spectra, *Phys. Rev. B*, **1997**, *55*, 10382 10391.

⁴¹ Chaboy, J.; Nakajima, N.; Tezuka, Y. Ab Initio X-ray Absorption Near-edge Struture Study of Ti K-edge in Rutile, *J. Phys.: Condens. Matter*, **2007**, *19*, 266206.

- ⁴² Rossi, T.C.; Grolimund, D.; Nachtegaal, M.; Cannelli, O.; Mancini, G.F.; Bacellar, C.; Kinschel, D.; Rouxel, J.R.; Ohannessian, N.; Pergolesi, D. et al. X-ray Absorption Linear Dichroism at the Ti *K* edge of Anatase TiO₂ Single Crystals, *Phys. Rev. B*, **2019**, *100*, 245207.
- ⁴³ Mardare, D.; Yildiz, A.; Apetrei, R.; Rambu, P.; Florea, D.; Gheorge, N.G.; Macovei, D.; Teodorescu, M.; Luca, D. The Meyer-Neldel Rule in Amorphous TiO₂ Films with Different Fe Content, *J. Mater. Res.* **2012**, *27*, 2271-2277.
- ⁴⁴ Fracchia, M.; Ghigna, P.; Minguzzi, A.; Vertova, A.; Turco, F.; Cerrato, G.; Meroni, D. Role of Synthetic Parameters on the Structural and Optical Properties of N, Sn-Copromoted Nanostructured TiO₂: A Combined Ti K-edge and Sn L_{2,3}-edges X-ray Absorption Investigation, *Nanomaterials*, **2020**, *10*, 1224; doi:10.3390/nano10061224.
- ⁴⁵ Kim, J.Y.; Rodriguez, J.A.; Hanson, J.C.; Frenkel, A.I.; Lee, P. L. Reduction of CuO and Cu₂O: H Embedding and Kinetic Effects in the Formation of Suboxides, *J. Am. Chem. Soc.* **2003**, *125*, 10684-10692.
- ⁴⁶ Unutulmazsoy, Y.; Cancellieri, C.; Lin, L.; Jeurgens, L.P.H. Reduction of Thermally Grown Single-phase CuO and Cu₂O Thin Films by In-situ Time-resolved XRD, *Applied Surf. Sci.* **2022**, *588*, 152896.
- ⁴⁷ Sun, X.; Wu, D.; Zou, L.; House, S.D.; Chen, X.; Li, M.; Zakharov, D.N.; Yang, J.C.; Zhou, G. Dislocation-induced Stop-and-go Kinetics of Interfacial Transformations. *Nature*, **2022**, *607*, 708-713.
- ⁴⁸ Wang, Q.; Hanson, J.C.; Frenkel, A.I. Solving the Structure of Reaction Intermediates by Time-resolved Synchrotron X-ray Absorption Spectroscopy, *J. Chem. Phys.* **2008**, *129*, 234502.
- ⁴⁹ Xu, F.; An, W.; Baber, A.E.; Grinter, D.C.; Senanayake, S.D.; White, M.G.; Liu, P.; Stacchiola, D.J. Enhanced Oxide Reduction by Hydrogen at Cuprous Oxide–Copper Interfaces near Ascending Step Edges, *J. Phys. Chem. C*, **2022**, *126*, 18645–18651.
- ⁵⁰ Dahl, M.; Liu, Y.; Yin, Y. Composite Titanium Dioxide Nanomaterials, *Chem. Reviews*, **2014**, *114*, 9853-9889.
- ⁵¹ Etape, E.K.; Ngolui, L.J.; Foba-Tendo, J.; Yufanyi, D.M.; Namondo, B.V. Synthesis and Characterization of CuO, TiO₂, and CuO-TiO₂ Mixed Oxide by Modified Oxalate Route, *J. Applied Chem.* **2017**, 4518654.
- ⁵² Eren, B.; Weatherup, R. S.; Liakakos, N.; Somorjai, G. A.; Salmeron, M. Dissociative Carbon Dioxide Adsorption and Morphological Changes on Cu(100) and Cu(111) at Ambient Pressures. *J. Am. Chem. Soc.* **2016**, *138*, 8207-8211.

⁵³ Hagman, B.; Posada-Borbon, A.; Schaefer, A.; Shipilin, M.; Zhang, C.; Merte, L.R.; Hellman, A.; Lundgreen, E.; Grönbeck, H.; Gustafson, J. Steps Control the Dissociation of CO₂ on Cu(100). *J. Am. Chem. Soc.* **2018**, *140*, 12974-12979.

- ⁵⁴ Hadden, R. A.; Vandervell, H. D.; Waugh, K. C.; Webb, G. The Adsorption and Decomposition of Carbon Dioxide on Polycrystalline Copper. *Catalysis Letters* **1988**, *1*, 27-33.
- ⁵⁵ Huygh, S.; Bogaerts, A.; Neyts, E.C. How Oxygen Vacancies Activate CO₂ Dissociation on Anatase TiO₂(101), *J. Phys. Chem. C*, **2016**, *120*, 21659-21665.
- ⁵⁶ Yan, P.; Han, Y.; Xu, Q. CO₂-Induced Two-Dimensional Amorphous TiO₂ and Its Excellent Film-Forming Properties, *ChemNanoMat*, **2022**, *8*, e202200216.
- ⁵⁷ Huygh, S.; Bogaerts, A.; Neyts, E.C. How Oxygen Vacancies Activate CO₂ Dissociation on Anatase TiO₂(101), *J. Phys. Chem. C*, **2016**, *120*, 21659-21665.
- ⁵⁸ Hendriksen, B., Influence of Atomic Structure, Steps, and Kinks on the Catalytic Activity: In Situ Surface Studies, in: *Current Trends of Surface Science and Catalysis*, Edited by J. Park, vol 1, pp. 171-195, Springer, New York, 2014.
- ⁵⁹ Zaera, F. Nanostructured Materials for Applications in Heterogeneous Catalysis, *Chem. Soc. Rev.* **2013**, *42*, 2746-2762.
- ⁶⁰ Rui, N.; Wang, X.; Deng, K.; Moncada, J.; Rosales, R.; Zhang, F.; Xu, W.; Waluyo, I.; Hunt, A.; Stavitski, E.; et al. Atomic Structural Origin of the High Methanol Selectivity over In₂O₃– Metal Interfaces: Metal–Support Interactions and the Formation of a InO_x Overlayer in Ru/In₂O₃ Catalysts during CO₂ Hydrogenation. *ACS Catal.* **2023**, *13*, 3187-3200.
- ⁶¹ Crozier, P. A.; Hansen, T. W. In situ and Operando Transmission Electron Microscopy of Catalytic Materials. *MRS Bulletin* **2015**, *40*, 38-45.
- ⁶² Ciston, J.; Si, R.; Rodriguez, J.A.; Hanson, J.C.; Martínez-Arias, A.; Fernandez-García, M.; Zhu, Y. Morphological and Structural Changes during the Reduction and Reoxidation of CuO/CeO₂ and Ce_{1-x}Cu_xO₂ Nanocatalysts: In Situ Studies with Environmental TEM, XRD, and XAS. *J. Phys. Chem. C* **2011**, *115*, 13851-13859.
- ⁶³ Docherty, S.R.; Safonova, O.V.; Copéret, C. Surface Redox Dynamics in Gold–Zinc CO₂ Hydrogenation Catalysts, *J. Am. Chem. Soc.* **2023**, *145*, 13526-13530.
- ⁶⁴ Syzgantseva, O.; Gonzalez-Navarrete, P.; Calatayud, M.; Bromley, S.T.; Minot, C. Theoretical Investigation of the Hydrogenation of $(TiO_2)_N$ Clusters (N = 1-10). *J. Phys. Chem. C*, **2011**, *115*, 15890-15899.
- ⁶⁵ Bautista Hernandez, A.; Chigo Anota, E.; Severiano Carrillo, F.; Vazquez Cuchillo, O.; Salazar Villanueva, M. In-silico Study of the Adsorption of H₂, CO and CO₂ Chemical Species

- on $(TiO_2)_n$ n=15–20 Clusters: The $(TiO_2)_{19}$ Case as Candidate Promising, *J. Molec. Graph. and Bonding*, **2022**, 117, 108316.
- ⁶⁶ Wei, B.; Calatayud, M. Hydrogen activation on Anatase TiO₂: Effect of surface termination, *Catal. Today*, **2022**, *397-399*, 113-120.
- ⁶⁷ Surnev, S., Schoiswohl, J., Kresse, G., Ramsey, M. G. & Netzer, F. P. Reversible Dynamic Behavior in Catalyst Systems: Oscillations of Structure and Morphology. *Phys. Rev. Lett.* **2002**, *89*, 246101.
- ⁶⁸ Li, D.; Xu, F.; Tang, X; Tian,S.; Dai, S.; Pu, T.; Liu, X.; Tian, P.; Xuan, F; Zhi, X. et al. Induced Activation of the Commercial Cu/ZnO/Al₂O₃ Catalyst for the Steam Reforming of Methanol. *Nature Catal.* **2022**, *5*, 99–108.
- ⁶⁹ Trovarelli, A.; Llorca, J. Ceria Catalysts at Nanoscale: How Do Crystal Shapes Shape Catalysis? *ACS Catal.* **2017**, *7*, 4716-4735.
- ⁷⁰ Polo-Garzon, F.; Blum, T.F.; Bao, Z.; Wang, K.; Fung, V.; Huang, Z.; Bickel, E.E.; Jiang, D,; Chi, M.; Wu, Z. In situ Strong Metal-Support Interaction (SMSI) Affects Catalytic Alcohol Conversion, *ACS Catal.* **2021**, *11*, 1938-1945.
- ⁷¹ Hamlyn, R.C.; Mahapatra, M.; Grinter, D.C.; Xu, F.; Luo, S.; Palomino, R.M.; Kattel, S.; Waluyo, I.; Liu, P.; Stacchiola, D,J.; Senanayake, S.D.; Rodriguez, J.A. Imaging the ordering of a weakly adsorbed two-dimensional condensate: ambient-pressure microscopy and spectroscopy of CO₂ molecules on rutile TiO₂(110), *Phys. Chem. Chem. Phys.* **2018**, 20, 13122-13126.
- ⁷² Reddy, K.P.; Islam, A.; Tian, Y.; Lim, H.; Kim, J.; Kim, D.; Hunt, A.; Waluyo, I.; Rodriguez, J.A. MgO Nanostructures on Cu(111): Understanding Size- and Morphology-Dependent CO₂ Binding and Hydrogenation, *J. Phys. Chem. C*, **2024**, *128*, 7149–7158.
- ⁷³ Rietveld, H. A profile refinement method for nuclear and magnetic structures. *Journal of Applied Crystallography* **1969**, *2*, 65-71.
- ⁷⁴ Toby, B. H.; Von Dreele, R. B. GSAS-II: the genesis of a modern open-source all purpose crystallography software package. *Journal of Applied Crystallography* **2013**, *46*, 544-549.
- ⁷⁵ Nguyen, L.; Tang, Y.; Li, Y.; Zhng, X.; Wang, D.; Tao, F. Dual reactor for in situ/operando fluorescent mode XAS studies of sample containing low-concentration 3d or 5d metal elements. *Review of Scientific Instruments* **2018**, *89*, 054103.
- ⁷⁶ Ravel, B.; Newville, M. ATHENA, ARTEMIS, HEPHAESTUS: data analysis for X-ray absorption spectroscopy using IFEFFIT. *Journal of Synchrotron Radiation* **2005**, *12*, 537-541.
- ⁷⁷ De la Peña, Francisco; Prestat, E.; Fauske, V.T.; Burdet, P.; Lahnemann, J.; Jokubauskas, P.; Furnival, T.; Nord, M.; Oslasevicius, T.; MacAsthur, K.E.; Johnstone, D.N.; Sarahan, M.; Taillon, J.; Aarholt, T.; Migunov, V.; Eljarrat, A.; Caron, J.; Francis, C.; Nemoto, T.; Poon, T.; Mazzucco,

S.; Tappy, N.; Cautaerts, N.; Somnath, S.; Slater, T.; Walls, M.; Winkler, F.; Anes, H.W. Hyperspy/hyperspy: Release v1.7.3, https://zenodo.org/records/7263263

TOC

